A SUMMARY OF HINGELESS-ROTOR RESEARCH AT NASA - LANGLEY

John F. Ward and Robert J. Huston
Aerospace Engineer, VTOL Branch
Flight Mechanics and Technology Division
NASA Langley Research Center

Summary

35232

This paper will summarize the hingeless-rotor-research investigations conducted at the NASA Langley Research Center. These investigations include first, an exploratory flight-test program utilizing a three-blade hingeless rotor installed on an H-13 helicopter; and, second, the wind-tunnel testing of an aeroelastically scaled research model of a hingeless-rotor helicopter at simulated forward speeds up to 270 mph with full-scale Reynolds number and Mach number simulation. The third area of effort deals with the analytical treatment of the hingeless rotor. This work was done to define the fundamental reasons behind the results obtained in the experimental investigations.

The flight-test-program results illustrate the improved control power and damping characteristics of the hingeless-rotor system and the influence of the increased maneuverability on the rotor structural loads. The results of the dynamic model wind-tunnel investigation include a summary of the effect on structural loads and dynamics of reducing rotor blade chordwise stiffness to the level of the blade flapwise stiffness

Author

Notation

A_1	blade longitudinal cyclic pitch amplitude, radians
a_o	rotor coning angle, radians
B_1	blade lateral cyclic pitch amplitude, radians
$\bar{e}$	blade actual rigid offset, nondimensional
I	mass moment of inertia of blade about flapping hinge, slug-ft^2
K	pylon support sprag stiffness, lb/in.
K_ζ	effective spring stiffness at virtual lag hinge, in-lb/radian
M	total hub moment, ft-lb
M_A	longitudinal hub moment, ft-lb
M_B	lateral hub moment, ft-lb
M_{tip}	rotor advancing tip Mach number
q	aircraft pitching velocity, radians/sec
V	velocity along flight path, mph
V_{sim}	simulated full-scale velocity along flight path, mph
β_1	amplitude of blade first harmonic flapping angle with respect to shaft axis, radians
γ	blade Lock number
ζ	blade cyclic pitch amplitude, radians
θ_o	blade collective pitch angle, radians
θ_1	blade twist, radians
λ	inflow ratio
μ	rotor tip speed ratio
ω_{1s}	blade first bending mode, nonrotating, natural frequency, cpm
Ω	rotor rotational speed, rpm
Ω_N	normal operating rotor rotational speed, rpm

Introduction

The renewed interest in utilizing hingeless rotors on the helicopter stems from the potential advantages that may be achieved in three principal areas. First, because of cantilever action of the hingeless blade system, large aircraft control moments are transferred directly from the rotor into the fuselage as a strong source of aircraft pitching and rolling moment. This results in order-of-magnitude improvements in the controllability and flying qualities of the helicopter. The second area of improvement stems from the opportunity to achieve substantial reduction in rotor hub drag. This drag reduction comes about as a result of the aerodynamic cleanness that may be achieved by the elimination of flapping and lagging hinges, in-plane blade dampers, and associated hardware in the vicinity of the rotor hub. This reduction in complexity leads to a third area of improvement, which is a substantial reduction in mechanical maintenance.

The logical question that arises is: If the hingeless system looks so promising now, why has its development been postponed for so long? As pointed out in reference 1, some light can be shed on this question by considering a bit of history connected with an earlier nonarticulated or hingeless system. In 1939, Langley flight tested a nonarticulated, stiff bladed "rigid" rotor (ref. 2). One of the conclusions resulting from this investigation was that flexibility should be introduced into the system. It is believed that most and perhaps all past failures with "rigid" rotor systems involved attempts at preventing,

instead of incorporating, flexibility. Today's hingeless rotor designs do not attempt to avoid flexibility but, rather, varying amounts of flexibility are used as a means of alleviating high stress levels in the rotor system.

Most of the recent research and development of the hingeless rotor principle has been carried out by Lockheed Aircraft Corporation, Bell Helicopter Company, and NASA. Lockheed, which has chosen the hingeless-rotor helicopter as its entry into the helicopter field, is involved in the development of what is intended to be an optimized operational aircraft of this type (see ref. 3). Bell's work on the hingeless rotor (ref. 4) has involved the use of a number of experimental rotor systems installed on existing helicopters to provide research information.

Because of its potential for contributing to the solution of some existing limitations of the articulated rotor system and the need for understanding the fundamental advantages and restrictions of the hingeless system, NASA-Langley has undertaken a research program involving both flight and wind-tunnel investigations. The progress of this work has been reported in references 1, 5, 6, and 7. The present paper will summarize the results to date and present some of the general structural and dynamic characteristics of the hingeless-rotor system as determined from the flight and wind-tunnel investigations.

Flight Test

In order to begin exploratory flight-test work with a hingeless-rotor system, NASA purchased from Bell Helicopter Company a duplicate of an existing set of experimental hingeless-rotor components (see ref. 4). These rotor and control system components were installed on an Army-supplied H-13G helicopter and a flight-test program was carried out at Langley. The test aircraft is shown in figure 1. This aircraft was not intended to be an optimum design but was an available experimental vehicle which offered an opportunity to conduct a preliminary investigation of the hingeless-rotor concept.

During the program, data were obtained for various flight conditions throughout the forward-speed range. In addition to level-flight conditions data were obtained in autorotation, vertical descents, steep turns in level and autorotative flight, maneuvers, and slope takeoffs and landings.

Instrumentation

Since the principal innovation in the hingeless system is the ability to transfer large moments from the rotor system into the hub and rotor shaft, attention was focused on the measurement of the structural loads in this area. Details of the hub assembly are shown in figure 2. The blade root, hub, rotor shaft and control linkages were the primary components selected for strain-gage instrumentation. Flight-test instrumentation also included measurement of the aircraft's flying qualities. This instrumentation included capability for measurement of aircraft center-of-gravity linear accelerations; aircraft angular-velocities in roll, pitch and yaw; and pilot's control positions.

Control and Response

While the documentation of the aircraft's flying qualities was of secondary concern in this particular program, the aircraft control and response will be discussed first in order to describe the general behavior of the response to pilot control and in order to form a basis for the later discussion of the structural loads associated with the aircraft's response.

Measured response.- The favorable flying qualities of the hingeless rotor became quite obvious early in the flight program. A sample illustration of the improved characteristics is presented in figure 3. This figure, taken from reference 6, shows a time history of the aircraft's angular velocity in pitch produced by a longitudinal control step input. The response of the hingeless-rotor helicopter shown by the solid line is very rapid when compared to the response of an articulated rotor as indicated by the dashed line.

This improvement in aircraft response is far more significant than can be indicated in figure 3(a). As pointed out in reference 6, the time lag of the hingeless system, due to a ramp input in control, plus the time constant (the time required to reach 63 percent of the steady-state value) is of the order of two-tenths of a second. Because of the "tight" response of the hingeless system, the pilot receives early and clear evidence of the angular velocity developed by the control motion. In contrast, the sample articulated rotor response is such that the pilot must wait over 1 second before the resulting steady-state angular velocity is reached.

The measured control power and damping (in pitch) of the hingeless system is plotted in figure 3(b) relative to the handling-qualities boundaries of reference 8. The hingeless rotor H-13G fully meets the minimum requirements and, in fact, possesses control power and damping values an order of magnitude greater than conventional articulated rotors. Previous investigations by NASA to establish minimum desirable control and response characteristics (ref. 9) covered only the bottom corner of figure 3(b) shown as the lined and dotted areas. The calculated control power and damping of the H-13G hingeless rotor is also plotted in figure 3(b). This point was calculated, using the methods of reference 10, assuming no control washout. Actually, the H-13G control system had a nonlinear washout of control input which was a function of pylon deflection.

Another example of the improved flying qualities of this hingeless rotor is reflected in the fact that with no artificial stabilization devices nor a tail surface on the fuselage, the test rotor-fuselage combination was stable throughout the speed range. The response of the helicopter

to a pull-and-hold maneuver at 75 mph is shown in figure 4 for two different sprag mount stiffnesses. (The sprag mounts restrain the lower extremes of the rotor pylon which is essentially pivoted near the aircraft center of gravity.) The time history of the normal acceleration is seen to be concave downward within 2 seconds for the hard sprag mounts and within slightly over 2 seconds for the soft sprag mounts. A short-period oscillation appears to be slightly more pronounced for the hard sprag mounts than for the soft sprag mounts. The stable response to a pull-and-hold maneuver is believed to be at least partially due to the results of an effective spring constant between the swashplate and the pilot's control. The flexibility in the rotor mast coupled with the elastic restraints at the lower end of the rotor mast result in the control system having an effective spring between the control input and the swashplate. Miller has indicated the improved response characteristics theoretically obtainable by the use of "rigid rotors," or flapping offset (ref. 11) or the use of spring and dampers in the control system (ref. 12). The combination of a hingeless rotor (resulting in an effective offset of approximately 12 percent) and the effective spring in the control system has, in this case, resulted in a helicopter with angle-of-attack stability. The effect of a change in the sprag stiffness (or the control-system spring) has modified the stability characteristics.

Calculated control and damping moments.- It is frequently stated that the control-moment and damping-moment capability of the hingeless rotor may be achieved with an articulated rotor with sufficient flapping hinge offset. It may be of interest to note in passing that theoretical examination shows there is no such thing as an equivalent flapping-hinge offset which represents all characteristics of a hingeless blade. A comparison of the hub moments of the hingeless and articulated systems is shown in figure 5 as a function of blade offset. In figure 5(a) a comparison of the hub total control moment per radian of blade cyclic pitch is presented as a function of actual blade offset $\bar{e}$ for a fixed blade radius and a conventional blade stiffness. In calculating the hub moments for the hingeless rotor the simplified methods presented in reference 10 were used. This method utilizes an equivalent "virtual offset" hinged blade with a spring at the hinge which gives the approximate cantilever blade first flapwise bending mode shape and natural frequency. In order to clarify the terminology used in this paper it is pointed out that the hub moments in figure 5 are compared on the basis of "actual" rigid offset (the offset of the blade flapping hinge in the case of the articulated blade or the point of attachment of the cantilever blade in the case of the hingeless system). Therefore, once an actual offset was assigned to the cantilever blade an equivalent hinged system with additional "virtual" offset and spring restraint could be determined. It has been assumed that the effective thrust vector tilt of the hingeless and articulated rotors is of second order, remains constant, and is approximately equal for both types (ref. 10). The same presentation is used in figure 5(b) for rotor pitch angular velocity damping moment and damping cross-coupling moment.

Referring to figure 5, it can be seen that it would require approximately 15-percent offset for the articulated system to achieve the control- and damping-moment capability of the hingeless system with a zero offset. If equal values of offset are used for both systems, the hingeless rotor provides greater hub moment capability over the range of practical offset values. In other words, for any given offset hinged rotor design, the simple removal of the hinge, changing the blade fundamental mode from the pendulum mode to the cantilever first bending mode results in an increase in moment capability. This is equivalent to supplying an additional 10 to 15 percent of effective offset to the original hinged rotor. This increased moment capability is accomplished with the likely prospect of a decrease in hub drag and complexity.

The influence of blade structural stiffness on the control moment and damping capability of the hingeless system is illustrated in figures 6(a) and 6(b), respectively. The variation of rotor hub nondimensional longitudinal control moment per radian of blade lateral cyclic pitch and the rotor hub damping moment per unit pitch angular velocity are presented (left-hand plot in figs. 6(a) and 6(b)) as functions of rotor blade nonrotating first-mode flapwise bending-frequency ratio ω_{1s}/Ω. Curves are presented for three values of blade Lock number (which represents blade density). These calculations were based upon the use of an equivalent offset hinge blade with spring restraint at the hinge, which gave the cantilever first bending mode natural frequency and approximate mode shape (ref. 10). The cross coupling, or rolling moments, due to blade lateral cyclic pitch input and pitching velocity are shown in the right-hand plot of figures 6(a) and 6(b), respectively. Again the moments are shown as a function of blade nonrotating first-bending-mode frequency ratio.

A successful hingeless rotor can be expected to have a frequency ratio of 0.2 or less, which is approximately that of the first cantilever bending mode of current articulated rotor blade designs. Higher values of ω_{1s}/Ω result in high bending stresses at the blade root because of lack of the centrifugal relief on a very stiff blade. Also as indicated in figure 6 there would be excessive cross coupling of hub moments. The cross coupling associated with blade lateral cyclic pitch input can be eliminated by proper mechanical phasing of control input; however, the reduction of the cross coupling of angular velocity damping presents a more difficult problem.

The simplest hingeless blade design approach would be to provide a flexible blade with the lowest value of ω_{1s}/Ω which would provide generous control power and damping capability with minimum cross coupling. The blade flapwise flexibility will allow for the centrifugal relief of large aerodynamic flapwise bending moments, thereby minimizing the blade flapwise bending stresses.

St ructural Loads

The general approach in the investigation was to sample all practical flight conditions in an effort to identify those conditions which required most immediate and detailed study of loads and dynamics. The structural loads data obtained during the flight program produced a number of interesting results. Prior to the flight program, it was anticipated that the stress levels in a number of structural components might be high and could perhaps limit the number of flight conditions investigated. For the most part, these high stress conditions did not materialize or could be avoided with proper pilot technique.

Ground operation.- With the aircraft resting on the ground the rotor-shaft stress levels were strongly dependent on piloting technique. The hingeless rotors have the capability for producing very high rolling and pitching moments (even with zero collective pitch) as a result of very small cyclic stick displacements. Therefore, during ground run-up and lift-off, extreme care had to be exercised by the pilot to keep the cyclic stick centered. It was necessary for the pilot to anticipate the cyclic trim position during the transition from the ground to airborne condition. In this case it was difficult to avoid high rotor-shaft cyclic stresses.

During slope landings and take-offs the situation was similar to the level ground condition but, in addition, it was necessary for the pilot to arrive at a level-attitude hover condition. This added to the difficulty of avoiding high rotor stress levels. However, it was determined that the best technique was to apply almost full collective control first to reduce the gear reaction on the ground prior to bringing the aircraft to a level attitude with cyclic control. The reverse control sequence was used in slope landings. In addition to pilot technique, there are a number of available approaches toward the reduction of this stress problem, but it will require specific design attention.

Flight loads.- The in-flight structural loads encountered are considered in two categories - first, those measured in level flight and, second, the loads measured in maneuvering flight.

The level-flight structural loads in primary rotor components are summarized in figure 7. Although the test rotor was fabricated from standard articulated components (except for the hub itself), the measured loads experienced in level flight throughout the speed range were not above the design "fatigue limit" for these components. "Fatigue limit" is defined as the cyclic load amplitude which results in a fatigue life equal to 10^8 cycles. Although the pitch link loads appear to be the largest in magnitude in figure 7, they were not considered to be unusually high. The maximum continuous cyclic pitch link loads during transition were on the order of ±80 pounds with a zero mean load. It is important to bear in mind, too, that the order of importance implied in figure 7 for the several components does not represent the overall results of this study.

During the test program, structural loads were monitored carefully as the flight envelope was expanded in order to assure safety of flight. As the program progressed, it became apparent that by utilizing the improved maneuver capability of the hingeless-rotor system high structural loads were induced. In general, the high loadings were not of a critical nature, and the increase in load level with severity of the maneuver was certainly not unexpected, especially with regard to rotor shaft and blade flapwise bending moments. However, the structural loading of most concern turned out to be the "in-plane" or chordwise bending moments induced in the rotor blades. The amplitude of the rotor blade-chordwise cyclic bending moment was very sensitive to maneuvers in which high aircraft angular velocities were developed. In some instances the amplitude of this loading expanded well beyond the structural fatigue limit, during pitch and roll maneuvers that were well within the capability of the aircraft. The buildup of cyclic chordwise bending moment with angular velocity occurred in pitch and roll maneuvers throughout the speed range. This is illustrated in figures 8 and 9 where sample time histories of the blade cyclic chordwise bending moments are presented for a hovering maneuver and a maneuver at a forward speed of 80 mph. The sample loads measurements presented in figure 8 (ref. 6) are for a hovering maneuver wherein the pilot executed a longitudinal control step displacement and recovery. During the period of maximum angular velocity, the buildup of the cyclic chordwise bending moments reaches a maximum of plus and minus 30 000 inch-pounds, which is above the structural fatigue limit of the blade. It should be pointed out that a large portion of the steady or mean chordwise bending moment (approximately 20,000 inch-pounds) for this rotor blade is due to the blade center-of-gravity axis being noncoincident with the neutral axis of the blade.

The oscillatory flapwise bending moment increases during the recovery maneuver, but does not show the degree of sensitivity to the maneuver exhibited by the chordwise bending moment. The flapwise bending moments are measured from the nonrotating droop load condition; thus the mean flapwise moment in flight is approximately a zero steady moment condition.

The rotating mast moments during the initial portion of the maneuver do not build up due to the application of a control moment because the initial control moment cancels a moment due to some minor center-of-gravity offset. However, during the recovery, where the control moment and the offset center-of-gravity moment add, the cyclic mast moments reach a maximum during maximum angular acceleration. It appears from this result that careful design consideration will be required to provide large allowable center-of-gravity travel in conjunction with full maneuver capability.

The situation at a forward speed of 80 mph in a 1.5g turn is shown in figure 9. Again the chordwise bending moment shows the large buildup with angular velocity, in this case to an amplitude of 35,000 inch-pounds, and again above the structural fatigue limit. Continuous operation at this load level would result in a 10-hour fatigue life for this rotor blade. In contrast to the loads measured in hovering and maximum forward-speed maneuver conditions are the loads measured during the maneuvers performed in autorotation starting at 50 mph. This case is shown in figure 10 and there is a complete lack of buildup in chordwise bending-moment amplitude during the maneuver, even though an angular velocity of 0.4 rad/sec was obtained.

This large change in chord load maneuver sensitivity with flight condition presented a very interesting situation which required an understanding of the fundamental factors involved. To understand this potential problem area an analytical treatment was undertaken. Theoretical analysis of the oscillatory chordwise bending moments during maneuver conditions was performed using an equivalent offset flapping hinge rotor with spring restraint. The results of this analysis indicated that for a given configuration the blade oscillatory chordwise bending moment buildup during maneuvers is primarily dependent upon chordwise stiffness, collective pitch, blade flapping, and coning deformation.

$$M_c = -K_\zeta \left[\gamma\left(\frac{\theta_o}{8} + \frac{\lambda}{3} + \frac{\theta_1}{10}\right) + 2a_o\right]\beta_1 \qquad (1)$$

Therefore, in this autorotation with low collective pitch and reduced flapping, the oscillatory moment during the maneuver would be predicted to be substantially reduced as was the actual case in figure 10.

As noted above, the amplitude of the blade chordwise bending moment is proportional to blade chordwise structural stiffness K_ζ, and this offers a means of alleviating the chord load sensitivity to maneuvers by reducing the blade chordwise stiffness. A demonstration of the feasibility of reducing blade structural loads by reduced chordwise stiffness will be included in the following discussion of hingeless-rotor dynamic model wind-tunnel test results.

Dynamic Model Investigation

As part of the hingeless-rotor research program, Langley has taken part in a cooperative effort involving U.S. Army-TRECOM, Lockheed Aircraft, and NASA. This program has involved the design, construction, and wind-tunnel testing of a 1/3-scale hingeless-rotor helicopter model, which was aeroelastically scaled. The program has proceeded in three phases. The first-phase testing was done in Langley 30-Foot by 60-Foot Full-Scale Tunnel and the second- and third-phase testing was done in the Langley 16-Foot Transonic Dynamics Tunnel. The initial results and analysis of the first- and second-phase testing will be published in reference 13.

A considerable number of dynamic configurations have been tested during the program. Research information of general interest resulting from the program includes complete structural load and aerodynamic data for the various rotor configurations. Rotors tested included those with twisted and untwisted blades; 3-, 4-, and 6-blade rotors; and variations in blade flapwise and chordwise stiffness and stiffness distribution. Each of these configurations was tested through a forward-speed and load-factor range simulating helicopter, unloaded rotor, and compound helicopter operation.

Model and Instrumentation

A schematic of the model and support system is shown in figure 11. The model rotor is 10 feet in diameter and the fuselage is supported on a soft spring mounting above the tunnel balance system. In the 16-Foot Transonic Dynamics Tunnel a special six-component strain-gage balance was used instead of the normal tunnel sting balance arrangement. In the Full-Scale-Tunnel testing the tunnel balance system was used. A 90-horsepower electric motor drive system was installed within the fuselage of the model and the model was restrained in yaw to provide the rotor antitorque moment. The model was essentially "flown" in the tunnel from a remote console where collective pitch, cyclic pitch, and model attitude control inputs were made.

In addition to the six-component balance data available, the model was fully instrumented to obtain structural loads, vibration, and control position data. This instrumentation included the following.

- Blade flapwise bending moments
- Blade chordwise bending moments
- Blade torsion
- Blade pitch position
- Pitch link loads
- Swashplate position
- Rotor shaft torsion
- Body accelerations (3 components)
- Body pitch and roll moment
- Body angle of attack

The balance data were recorded on punchcards and simultaneously all model instrumentation output was recorded on an oscillograph or magnetic tape.

Results

Phase I.- Seven rotor configurations were tested in the Langley 30-Foot by 60-Foot Full-Scale Tunnel. These tests covered a simulated speed range from hovering to 120 miles per hour and load factors up to 2.5.

A photograph of the model installation in the tunnel test section is shown in figure 12. The rotor configurations tested were all 3 bladed and

the blades were of wide chord giving a rotor solidity of 0.12. The testing in the Full-Scale Tunnel was done to study a variety of rotor dynamic configurations at low and moderate forward speeds prior to testing selected configurations at high forward speed in the Transonic Dynamics Tunnel. The model was properly scaled in all respects except Mach number and Reynolds number for the phase I testing.

Some of the highlights of the structural loads results are shown in figures 13, 14, and 15. In part (a) of each figure curves are shown for three rotor configurations in 1 g trimmed flight conditions. One configuration represents conventional blade design with a blade cantilevered from the rotor hub which had a very high chordwise stiffness relative to its flapwise stiffness. The second configuration was the same blade with a reduced chordwise stiffness at the root achieved by using a flexible drag link. The stiffness of the drag link was such that the static deflection of the blade tip under a tip load was equal in both the flapwise and chordwise direction. The third configuration was a blade in which the chordwise structural stiffness along the entire blade was equal to the flapwise blade stiffness.

The variation in oscillatory blade torsional load throughout the speed range is shown in figure 13(a). The corresponding variation in the magnitude of cyclic flapwise bending moment is shown in figure 14(a). In this case the first harmonic content of the flapwise moment was subject to some inaccuracy at the higher speeds due to the model being slightly out of trim.

From the standpoint of structural loads, the most significant result of the phase I testing is shown in figure 15(a) which shows the amplitude of cyclic chordwise moment at the blade root for 1 g flight over the simulated speed range. As indicated in the figure there is a large increase in chordwise cyclic load with increasing speed for the conventional blade (that is, for a blade with high chordwise stiffness and low flapwise stiffness). The chordwise stress levels reached on the conventional blade were excessive for continuous operation. By using a flexible drag link at the blade root to reduce the blade chordwise stiffness to match the flapwise stiffness a large reduction in chordwise cyclic loading was obtained over the entire speed range. An even greater reduction in the loads was achieved by matching the chordwise stiffness to the flapwise stiffness along the entire blade. Here again the introduction of flexibility has led to load reduction and this method of reducing chordwise loading shows promise of offering the solution to the problem of high cyclic chordwise moments experienced in the flight-test maneuvers mentioned in the first part of this paper (figs. 8 and 9). As indicated in equation (1) and demonstrated in the wind-tunnel-test results the blade chordwise stiffness K_ζ is a primary factor in determining the magnitude of the chordwise cyclic loading.

While the results presented in part (a) of figures 13, 14, and 15 are for 1 g flight, the effects of variations in load factor were investigated and the results are presented in part (b) of figures 13, 14, and 15. As indicated in figure 15(b), large reductions in blade chordwise cyclic loading were again obtained with the introduction of chordwise flexibility

Phase II.- Following completion of the model tests in the Full-Scale Tunnel at simulated forward speeds up to 120 mph, the model was tested in the Langley 16-Foot Transonic Dynamics Tunnel. In these tests the model was rebalanced and tested in Freon at a density of 0.008 slug per cubic foot and complete dynamic and aerodynamic scaling was achieved including Mach number and Reynolds number similitude. The model is shown installed in the Transonic Dynamics Tunnel in figure 16. The basic configuration tested was the 3-blade rotor with matched root stiffness. Aerodynamic and structural load data were obtained with simulated forward speeds from 60 to 240 mph and tip Mach number up to 0.92. Helicopter, unloaded rotor, and compound helicopter modes of operation were sampled. Chordwise cyclic load data obtained are shown in figure 17. This figure also includes the corresponding data obtained in the Full-Scale Tunnel (fig. 15) for comparison purposes. A beneficial influence of blade twist is also indicated in this figure. This beneficial influence of blade twist on chordwise cyclic load was also noted at the higher forward speed runs during the Full-Scale Tunnel tests of twisted and untwisted conventional blades.

Due to the fact that the rotor had been designed to enable wide variations in dynamic characteristics, a mechanical configuration resulted which was aerodynamically unsuitable and in some configurations had excessive structural damping; therefore the data for the phase II testing were not representative of an optimized design. Therefore, the third phase of testing was undertaken to obtain refined dynamic and aerodynamic information at more extreme conditions.

Phase III.- In the third phase, which was recently completed, the model was again tested in the Transonic Dynamics Tunnel. The blade and rotor hub design was optimized for low drag and the blades were of more conventional aspect ratio and the blade flapwise and chordwise stiffness were approximately matched along the entire blade. Rotors with 3, 4, and 6 blades were tested with rotor solidities of 0.06, 0.08, and 0.12, respectively. The 3- and 4-blade model configurations are shown in figures 18 and 19. The four-blade model was considered as the basic test configuration. As in the previous tests, structural loads and performance data were obtained for a range of load factors and forward speeds in the helicopter and unloaded rotor mode of operation. The following listing represents the maximum operating conditions reached in the unloaded rotor configuration for the 4-blade rotor configuration.

V_{sim}	$\frac{\Omega}{\Omega_n}$	M_{tip}	μ
258	1.0	0.95	0.58
272	.85	.88	.72
266	.71	.79	.85

Ω_n = normal simulated helicopter operating rotor speed

The data obtained in the third phase of testing are currently being reduced and analyzed, and are to be reported in the future; however, from the preliminary results noted as the test proceeded, the "optimized" rotor design with the low chordwise stiffness blades showed considerable promise from the standpoint of structural loads, vibration, and performance. This is not intended to imply that all problems have been satisfactorily solved, but rather that the hingeless rotor has been successfully operated at conditions which were more extreme in regard to combined dynamic pressure and Mach number than any known tests in the past.

Additional observations - One of the areas which requires careful investigation in reference to the reduced chordwise stiffness blade design is the ground resonance phenomenon. Due to the fact that the blade "in-plane" first bending mode natural frequency falls below normal operating rotor speed, a coupling of the in-plane blade oscillation with body pitch or roll oscillation may occur during run-up or shutdown of the rotor. This problem is the dynamic equivalent of classical "ground resonance" experienced with hinged rotor systems. The solution in the case of the hinged system required the addition of blade lag dampers and landing-gear dampers to stabilize the coupled oscillations of the rotor and body.

An extensive theoretical analysis of the ground resonance phenomenon for the hingeless rotor has been carried out in reference 14. This analysis included rotor aerodynamics; the results of this work, presented in reference 15, indicate that the coupled vibration mode can be stabilized without addition of artificial damping. During the third phase of model testing in the Transonic Dynamics Tunnel, limited ground resonance testing was conducted in air with the model ballasted for testing in Freon. This resulted in a dynamic simulation where aerodynamic forces were diminshed by approximately 60 percent. Under these conditions, cases of unstable "ground resonance" were encountered. In order to assure safe operation in the tunnel the body pitch and roll frequencies were adjusted to eliminate unstable resonance when operating in air. Operation still involved passing through a body pitch frequency at low rotor speed, which theoretically represented a ground resonant condition. Subsequent operation in Freon was carried out without experiencing unstable ground resonance. A thorough study of the ground resonance problem was not undertaken during the tunnel program to determine, experimentally, the role of rotor aerodynamics, blade stiffness, and control feedback; however, work of this type is tentatively being planned using the hingeless-rotor dynamic model.

Concluding Remarks

In general, the flight-research and wind-tunnel investigations carried out to date on the hingeless-rotor principle have been very encouraging and have indicated definite promise of improvements to be obtained by proper application of the principle. The hingeless-rotor system will undoubtedly be subject, in some degree, to many of the problems faced by the various articulated rotor systems in addition to some problems of its own. There are many ways open to cope with these problems with proper design attention based upon sufficient research information. Therefore, research investigations to completely define the advantages and limitations of the principle, and solutions to problem areas should proceed in an orderly manner.

References

1. Gustafson, F. B., Powered-Lift Research at Langley Field. Presented at the Royal Aeronautical Society Rotorcraft Section Meeting, London, England, December 7, 1962.

2. Gustafson, F. B., Flight Tests of the Wilford XOZ-1 Sea Gyroplane. NACA unpublished paper, 1941.

3. Statler, W. H., Heppe, R. R., and Cruz, E. S., Results of the XH-51A Rigid Rotor Research Helicopter Program. American Helicopter Society Proceedings of the Nineteenth Annual National Forum, May 1-3, 1963, Washington, D.C., pp. 119-137.

4. Cresap, W. L., Rigid Rotor Development and Flight Tests. Presented at the IAS 30th Annual Meeting, New York, New York, January 22-25, 1962.

5. Gustafson, F. B., Helicopter Design and Capability Trends as Seen from a Research Viewpoint. Presented at the 1962 SAE National Aerospace Engineering and Manufacturing Meeting, Los Angeles, California, October 8-12, 1962.

6. Huston, Robert J., and Tapscott, Robert J., The Results of Some Wind Tunnel and Flight Studies with Helicopter at NASA. Presented at New York Academy of Sciences Conference on Vertical Take-Off and Landing Aircraft, New New York, New York, December 10-12, 1962.

7. Campbell, J. P., Status of V/STOL Research and Development in the United States. Presented at the Ninth AIAA Anglo-American Conference, Boston, Massachusetts - Montreal, Canada, October 17-22, 1963.

8. Anon., Military Specification - General Requirements for Helicopter Flying and Ground Handling Qualities. MIL-F-8501A, 1961.

9. Tapscott, Robert J., Helicopters and VTOL Aircraft: Criteria for Control and Response Characteristics in Hovering and Low Speed Flight. Aerospace Engineering, Volume 19, Number 6, June 1960.

10. Young, Dr. M. I., A Simplified Theory of Hingeless Rotors with Application to Tandem Helicopters. American Helicopter Society Proceedings of the Eighteenth Annual National Forum, May 2-4, 1962, Washington, D.C., pp. 38-45.

11. Miller, R. H., Helicopter Control and Stability in Hovering Flight. Journal Aeronautical Sciences, Aug. 1948, vol. 15, no. 8, pp. 453-472.

12. Miller, R. H., A Method of Improving the Inherent Stability of Helicopters. Journal Aeronautical Sciences, June 1950, vol. 17, no. 6, pp. 363-374.

13. Hanson, T. F., Investigation of Elastic Coupling Phenomena of High-Speed Rigid Rotor Systems. Army - TRECOM Technical Report 6[illegible] Submitted under contract DA 44-1[illegible] by Lockheed - California Company, [illegible] 1964.)

14. Kanno, J. S., and Lundgren, S., Equations of Motion for the Dynamic Analysis of a Hovering Rotor Including Gyro Control System. Lockheed California Company, LR 17185, June 1961. (Submitted under U.S. Army - TRECOM contract DA 44-177-TC-828.)

15. Kanno, J. S., and Lundgren, S., 10-Foot Rigid Rotor Model Basic Data and Results of Hovering Cyclic Stability Analysis. LR 16997, July 1963. (Submitted under U.S. Army - TRECOM contract DA 44-177-TC-828.)

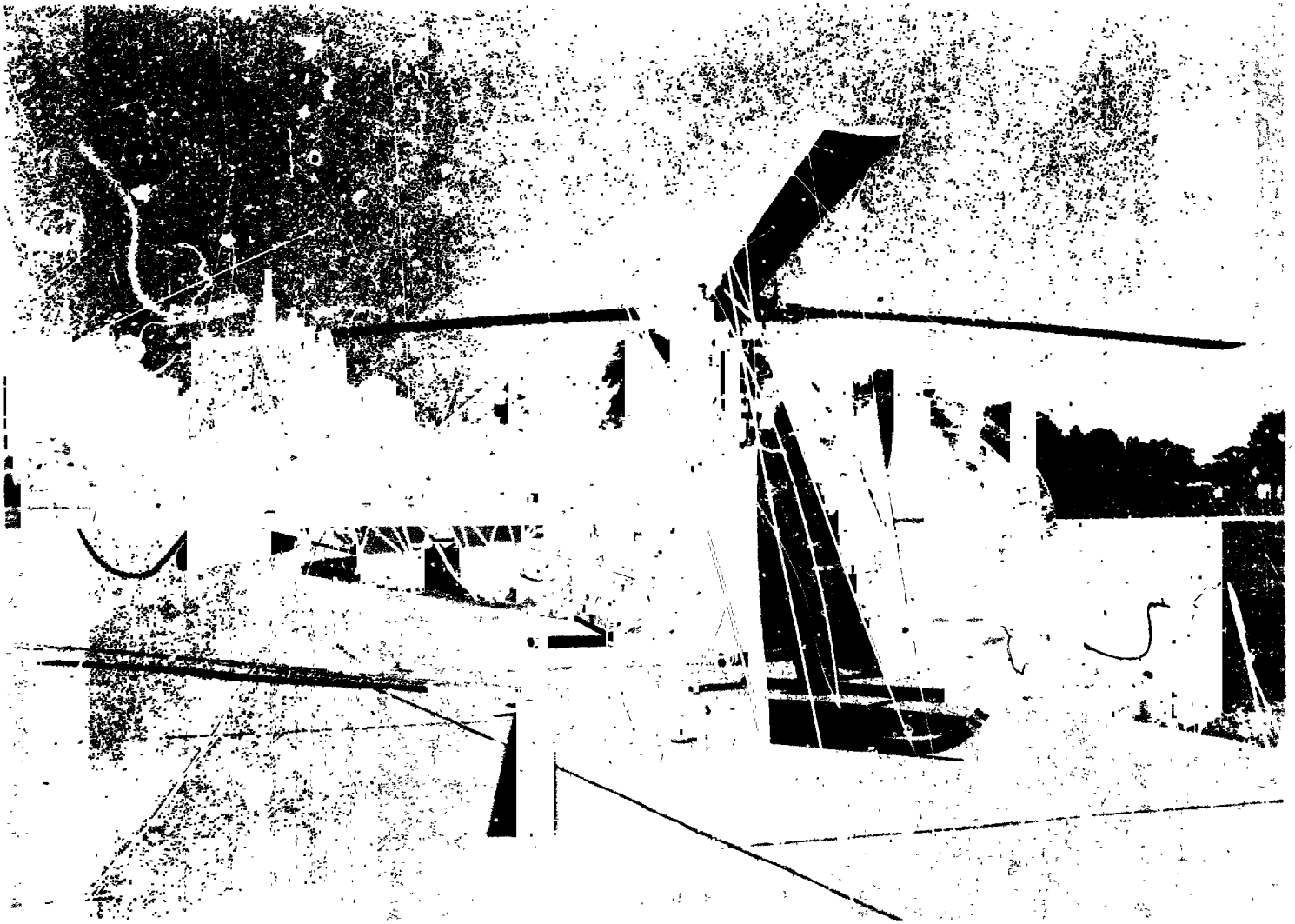

NASA

Figure 1.- Hingeless rotor on H-13G helicopter.

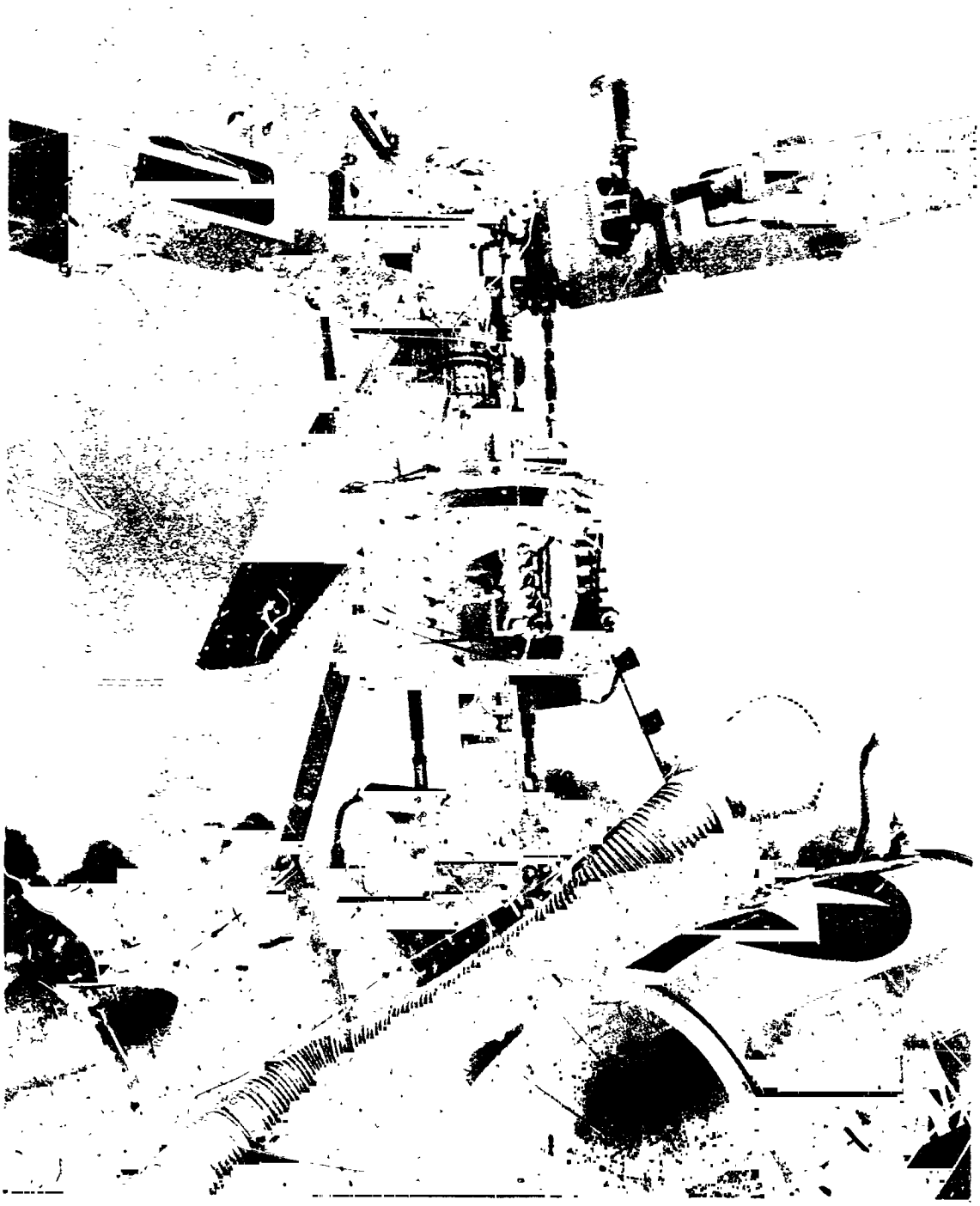

NASA

Figure 2.- Hingeless-rotor hub and slipring assembly.

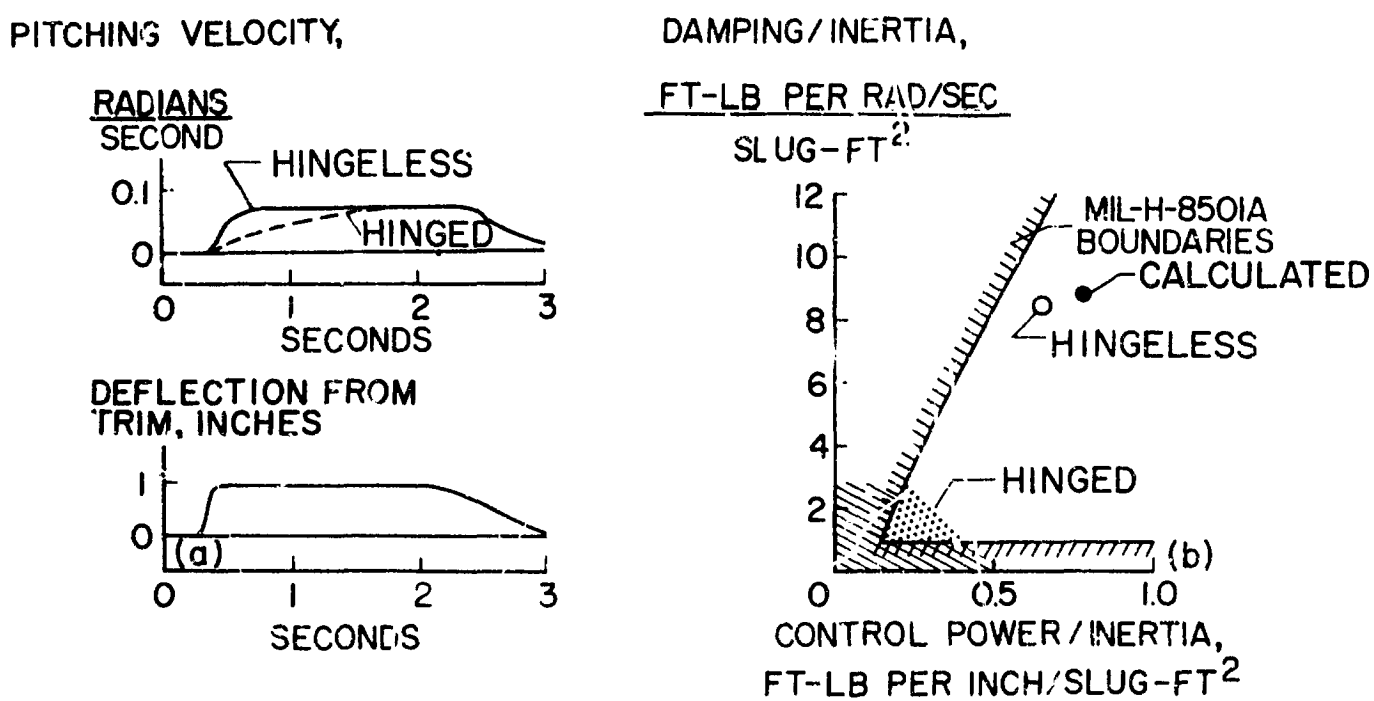

Figure 3.- Control-response and handling-qualities comparison of hingeless-rotor helicopter and conventional hinged-rotor helicopter in hovering flight.

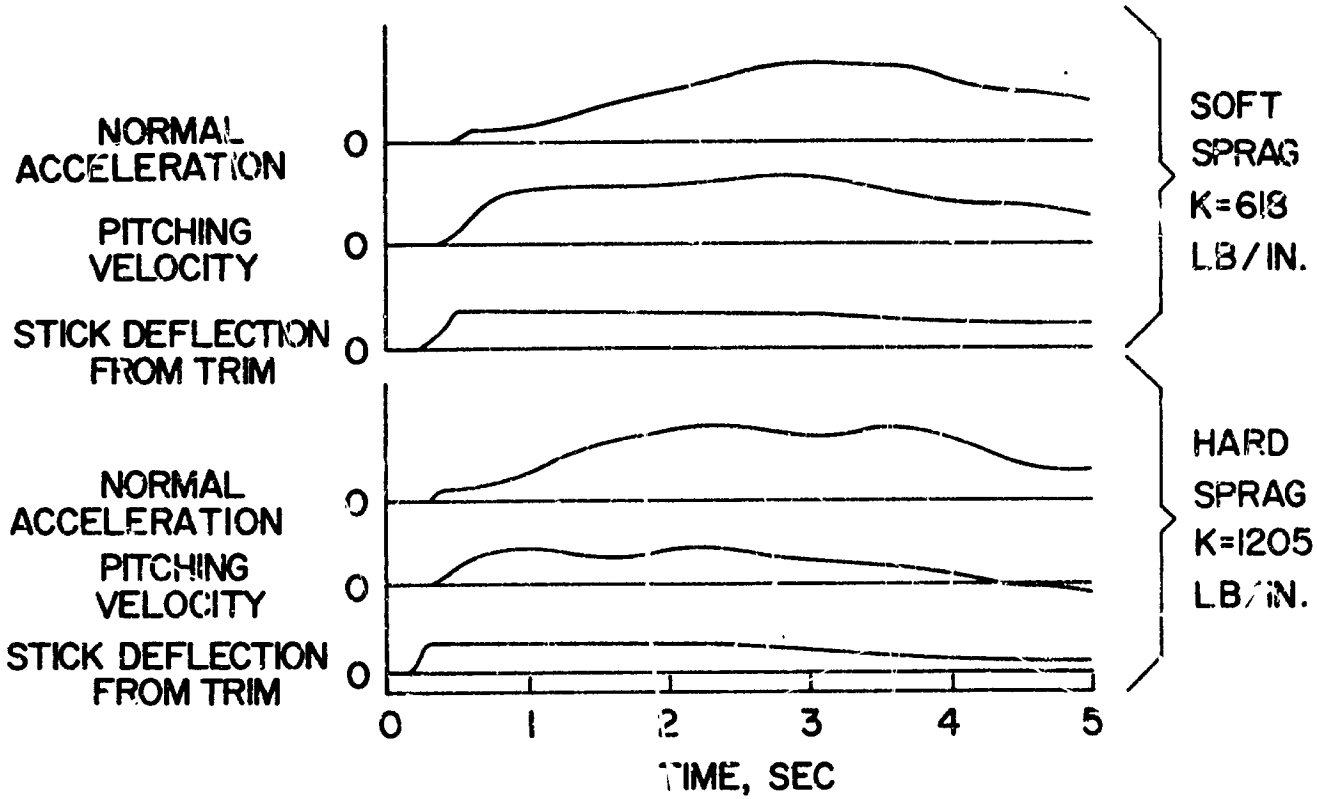

Figure 4.- Effect of pylon restraint stiffness on response to a pull and hold maneuver entered at 75 mph.

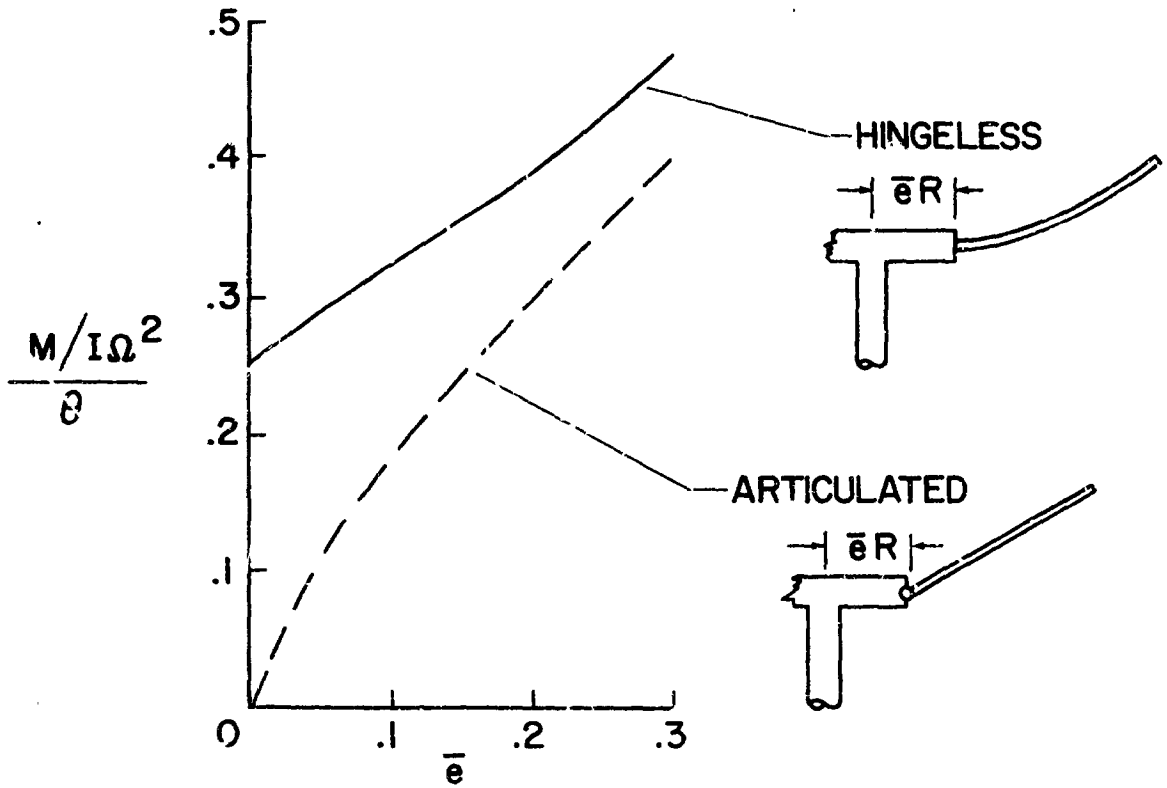

NASA

Figure 5(a).- Effect of offset on rotor hub total control moment per radian blade cyclic pitch angle. $\left(\frac{\omega_{1s}}{\Omega}\right)^2 = 0.06$.

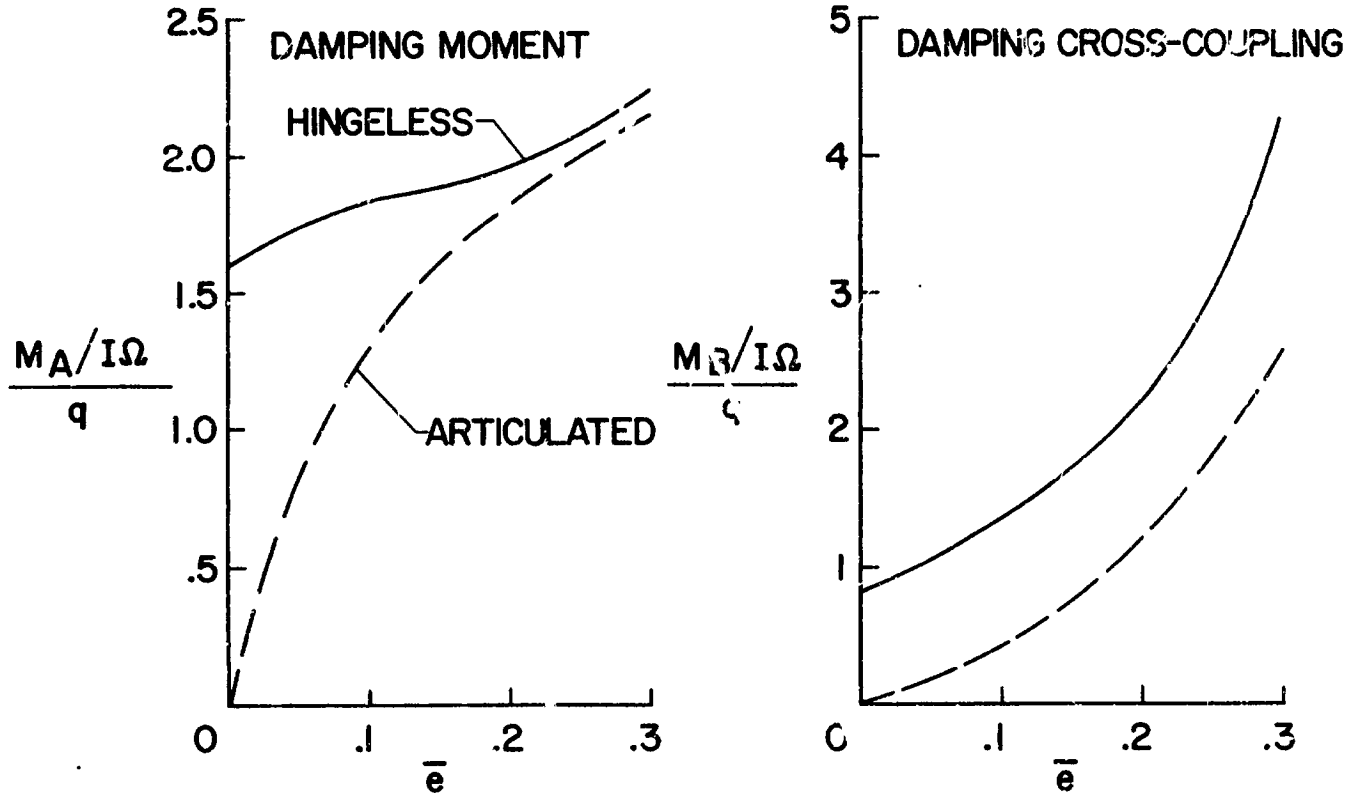

NASA

Figure 5(b).- Effect of offset on rotor hub damping moment and cross coupling. $\left(\frac{\omega_{1s}}{\Omega}\right)^2 = 0.06$.

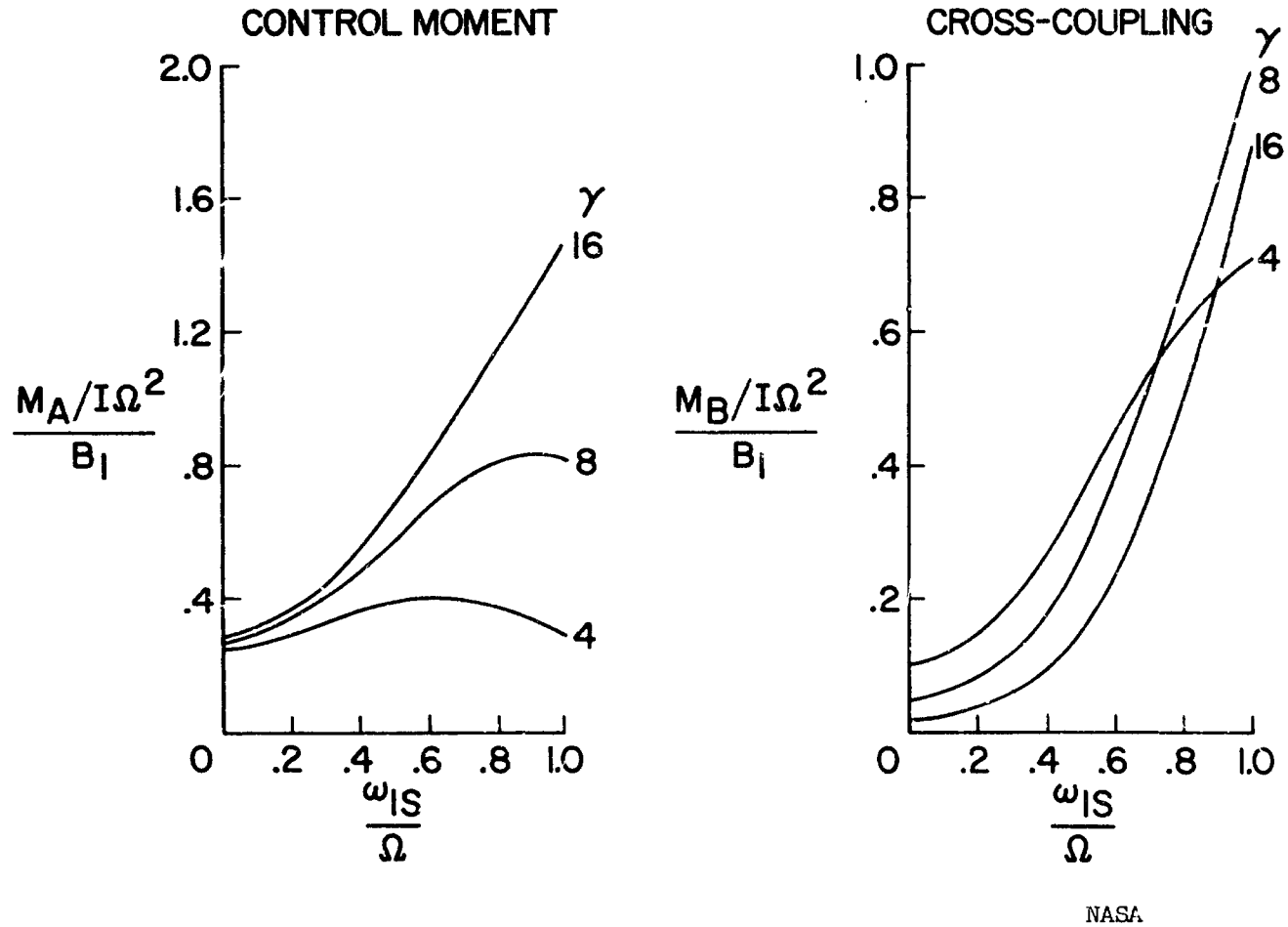

Figure 6(a).- Effect of blade stiffness on rotor hub control moment and cross coupling.

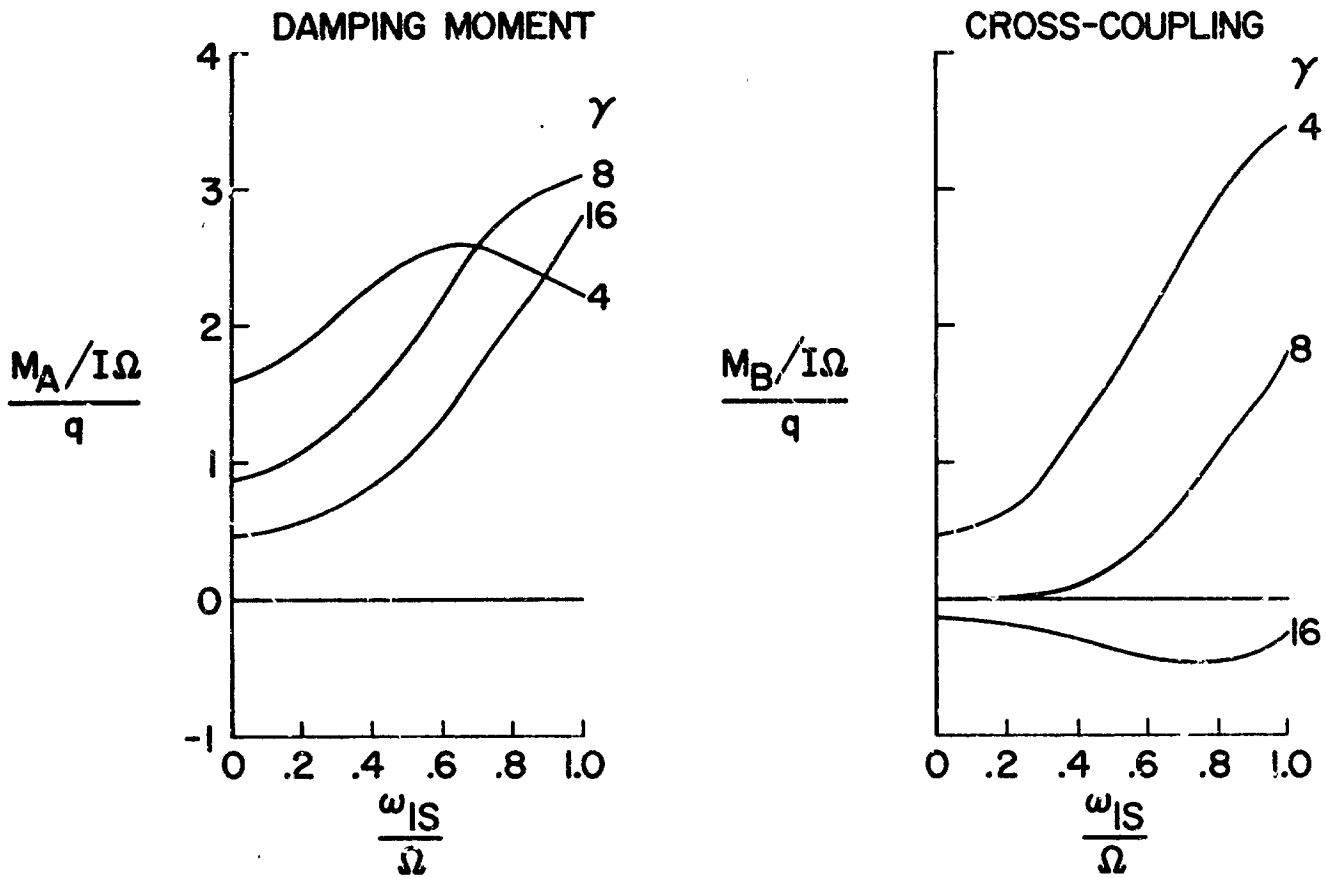

Figure 6(b).- Effect of blade stiffness on rotor hub damping moment and cross coupling.

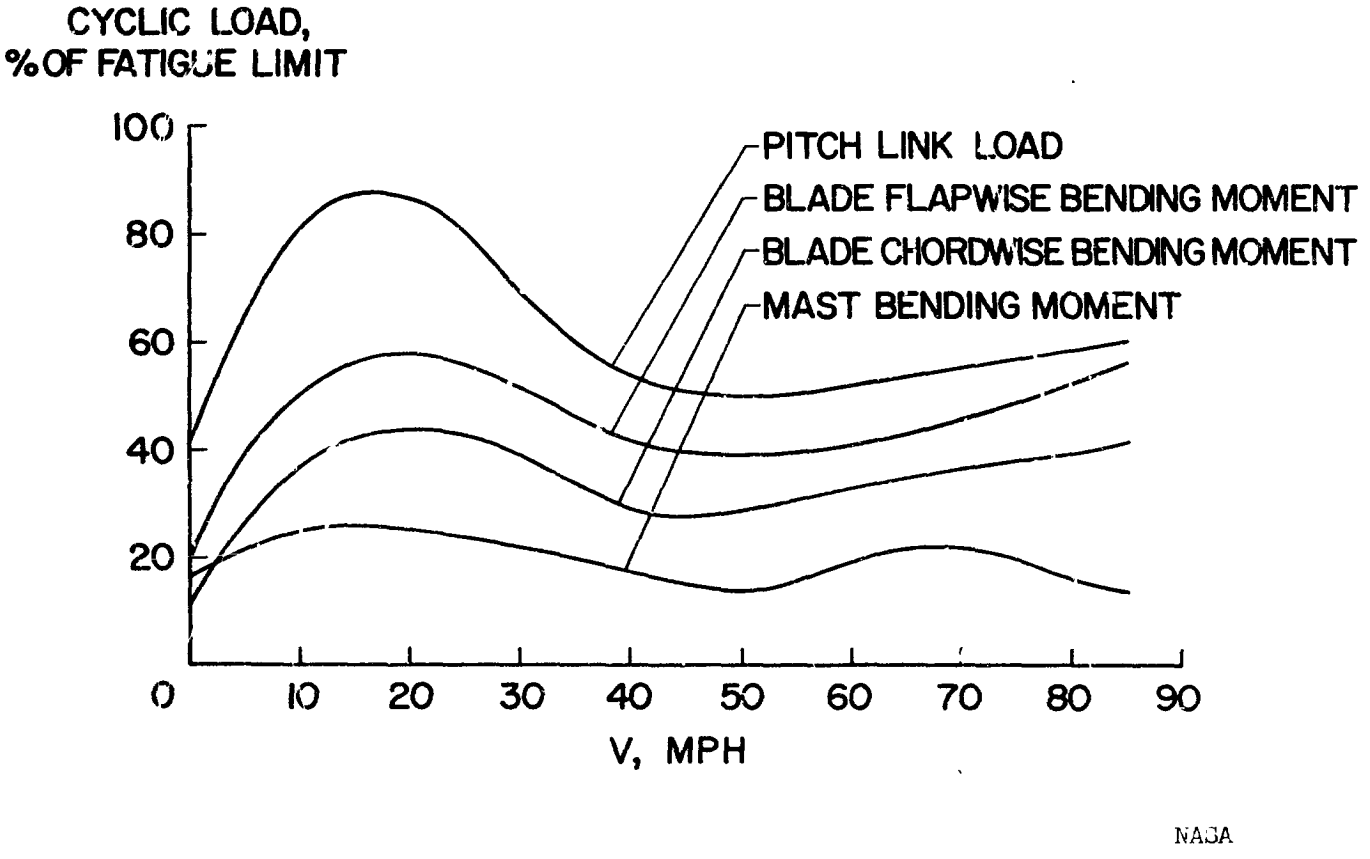

Figure 7.- H-13G hingless-rotor cyclic structural loads in level flight.

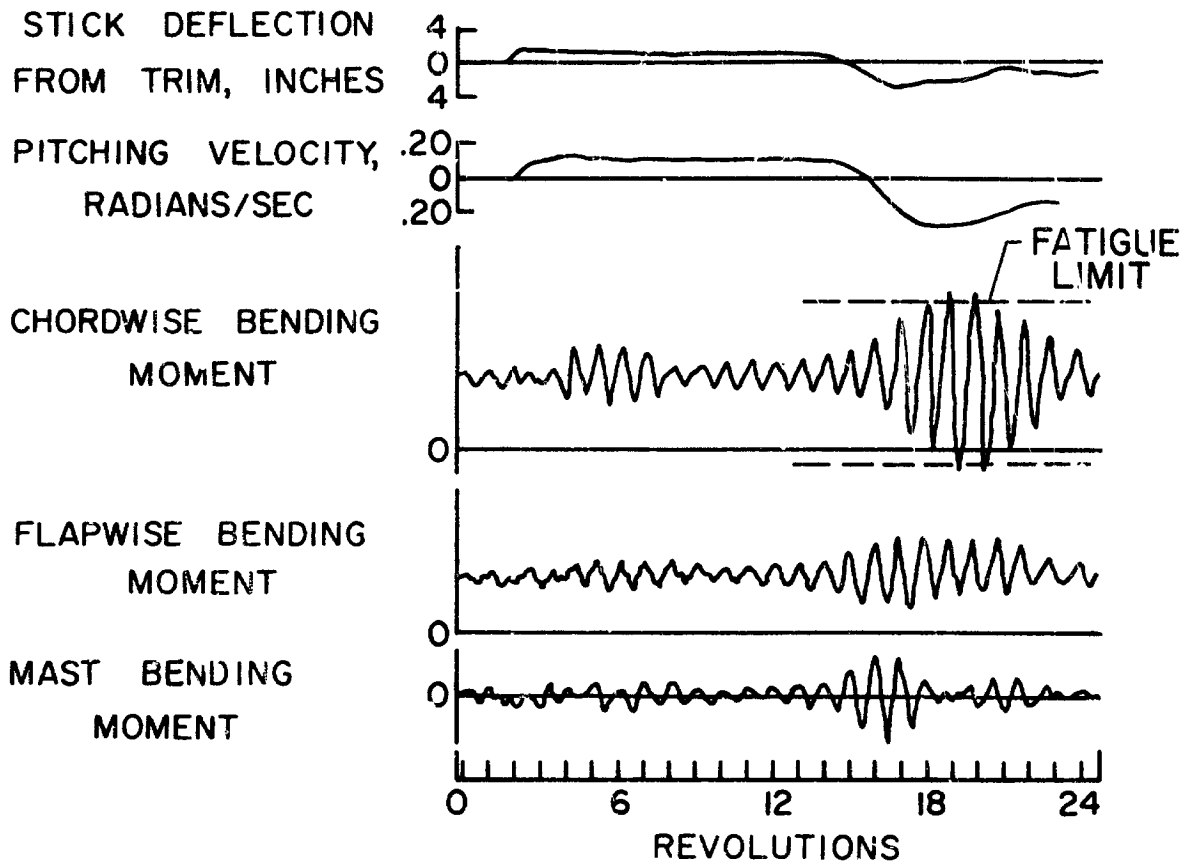

NASA

Figure 8.- Structural-loads time history during longitudinal maneuver and recovery with hingeless-rotor helicopter in hovering flight.

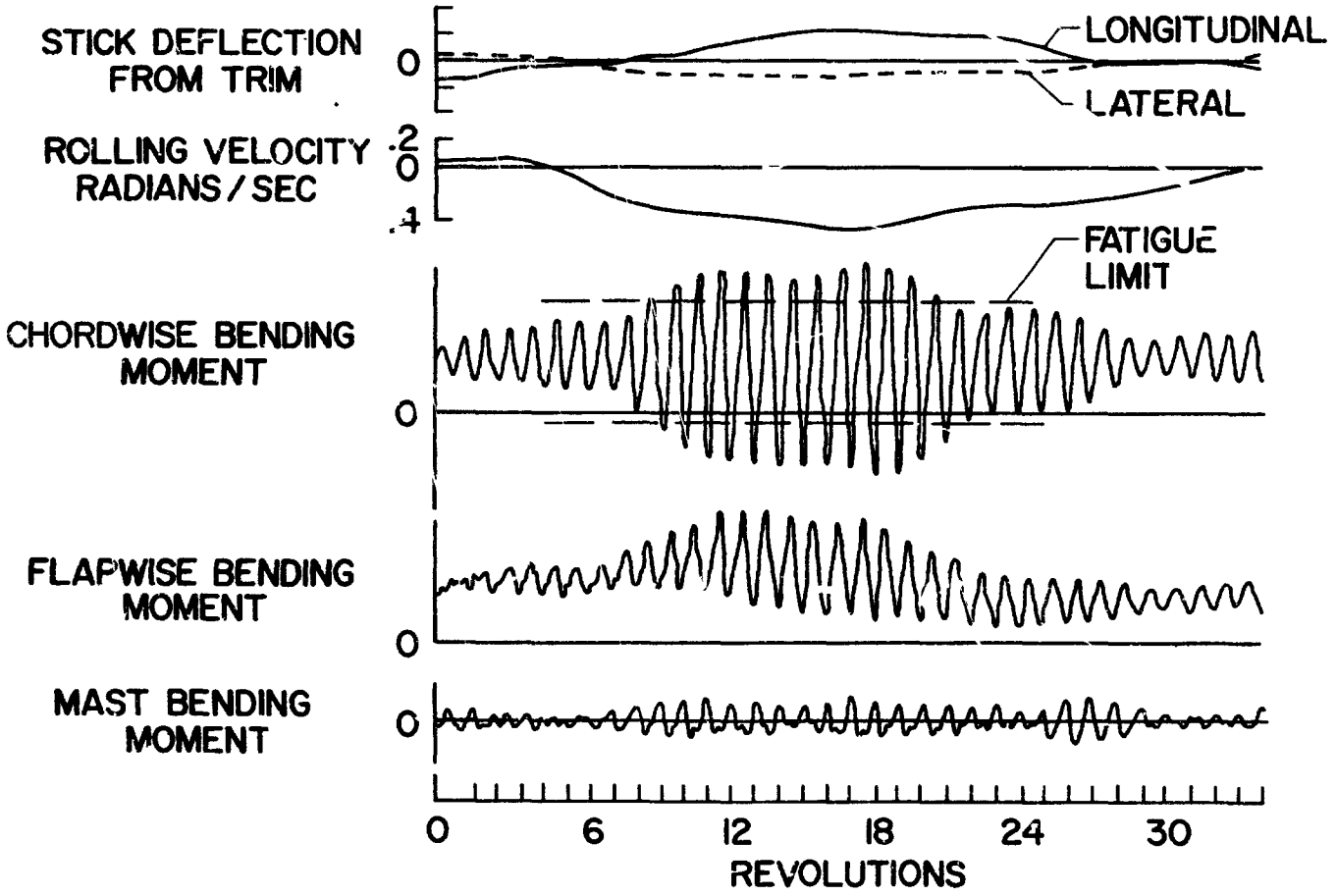

NASA

Figure 9.- Structural-loads time history during lateral maneuver with hingeless-rotor helicopter in level flight at a forward speed of 80 mph.

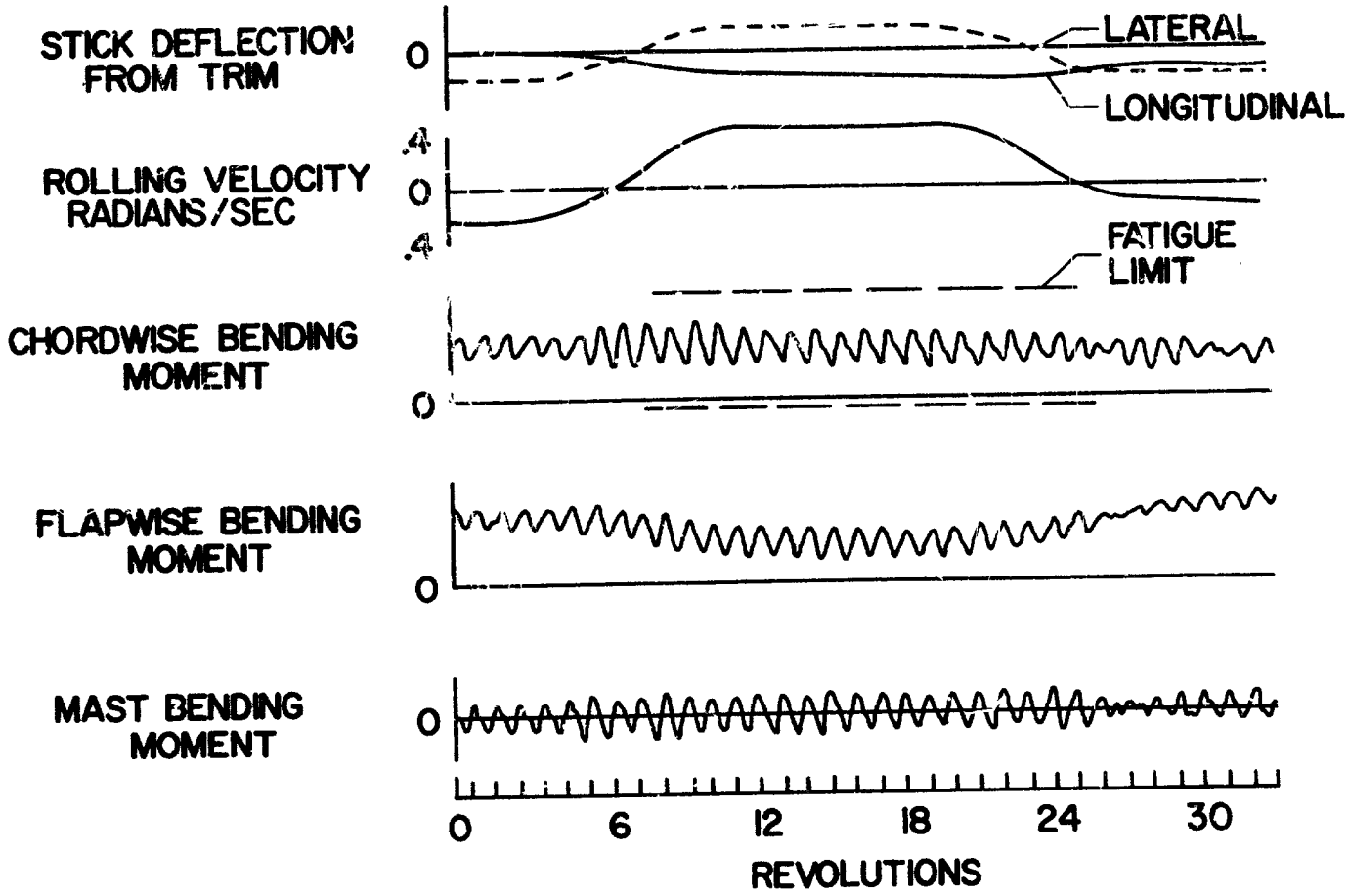

Figure 10.- Structural-loads time history during lateral maneuver with hingeless-rotor helicopter in autorotation. (Entry speed 50 mph.)

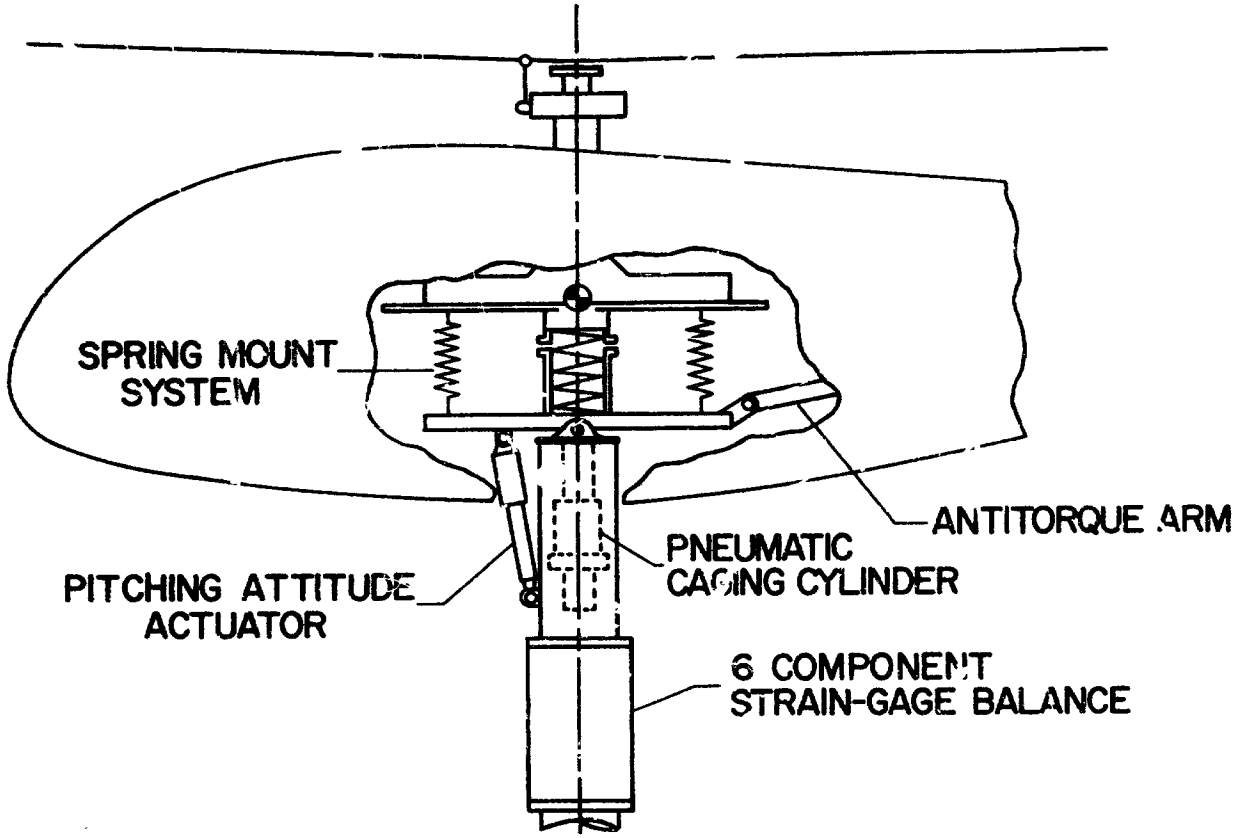

Figure 11.- Hingeless-rotor dynamic model support system in Langley 16-foot transonic dynamics tunnel.

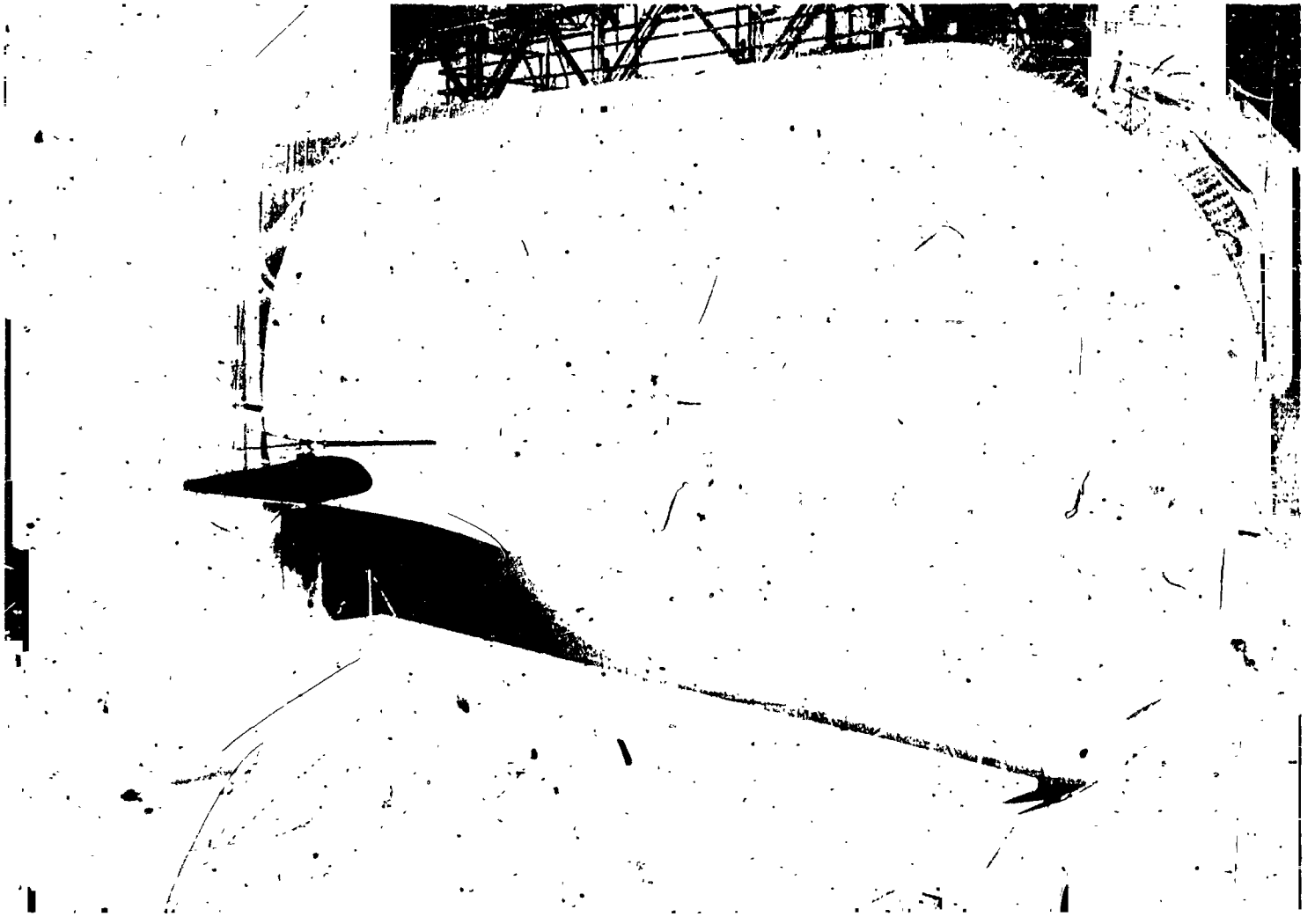

NASA

Figure 12.- Hingeless-rotor dynamic model in Langley 30-foot by 60-foot full-scale tunnel.

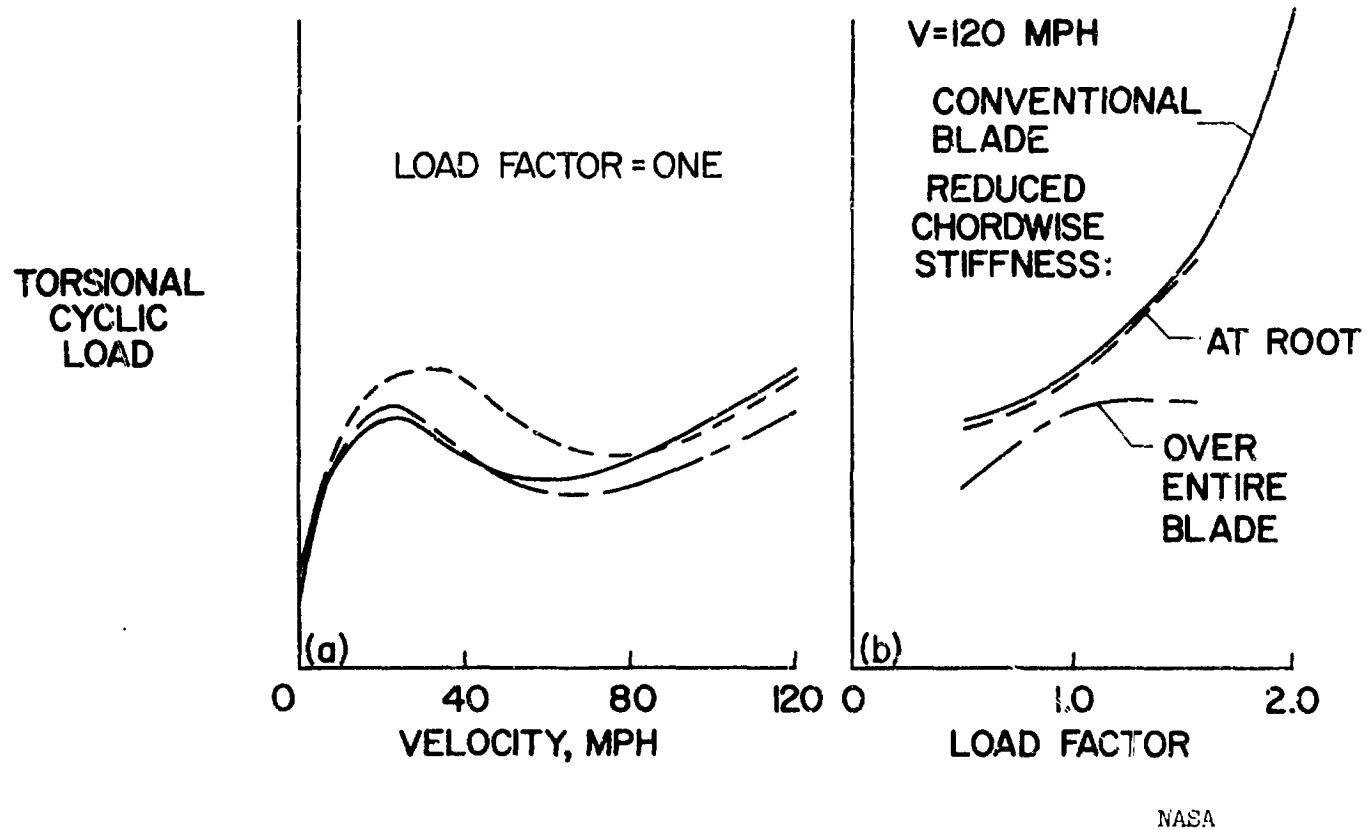

Figure 13.- Effect of blade chordwise stiffness on blade torsional cyclic load.

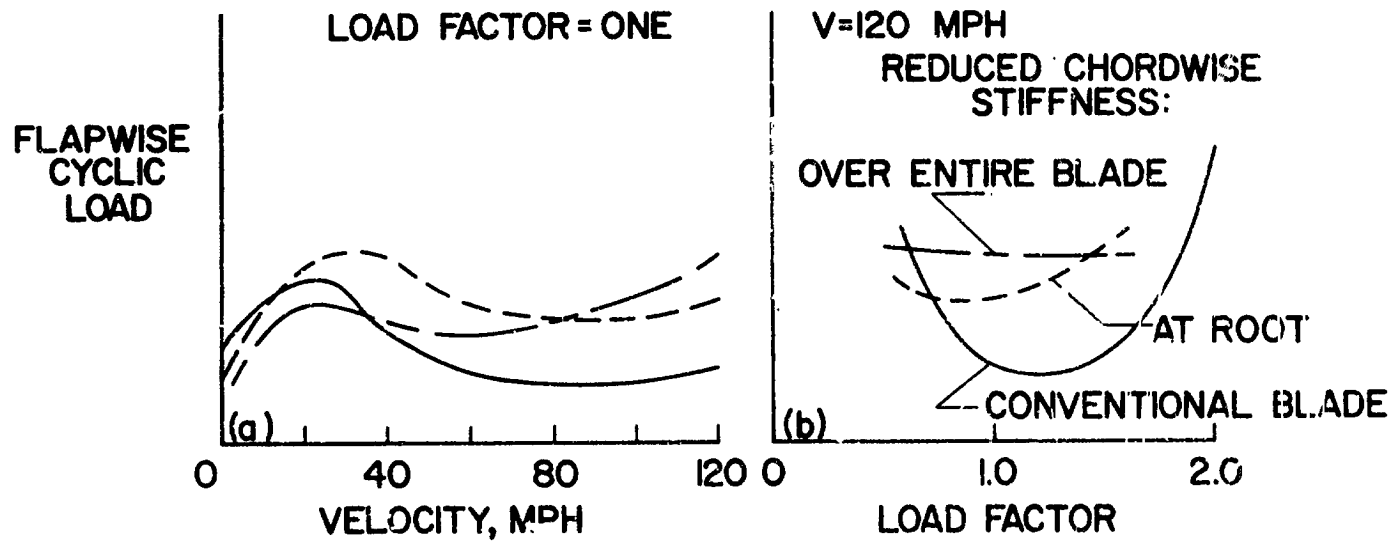

NASA

Figure 14.- Effect of blade chordwise stiffness on blade flapwise cyclic load.

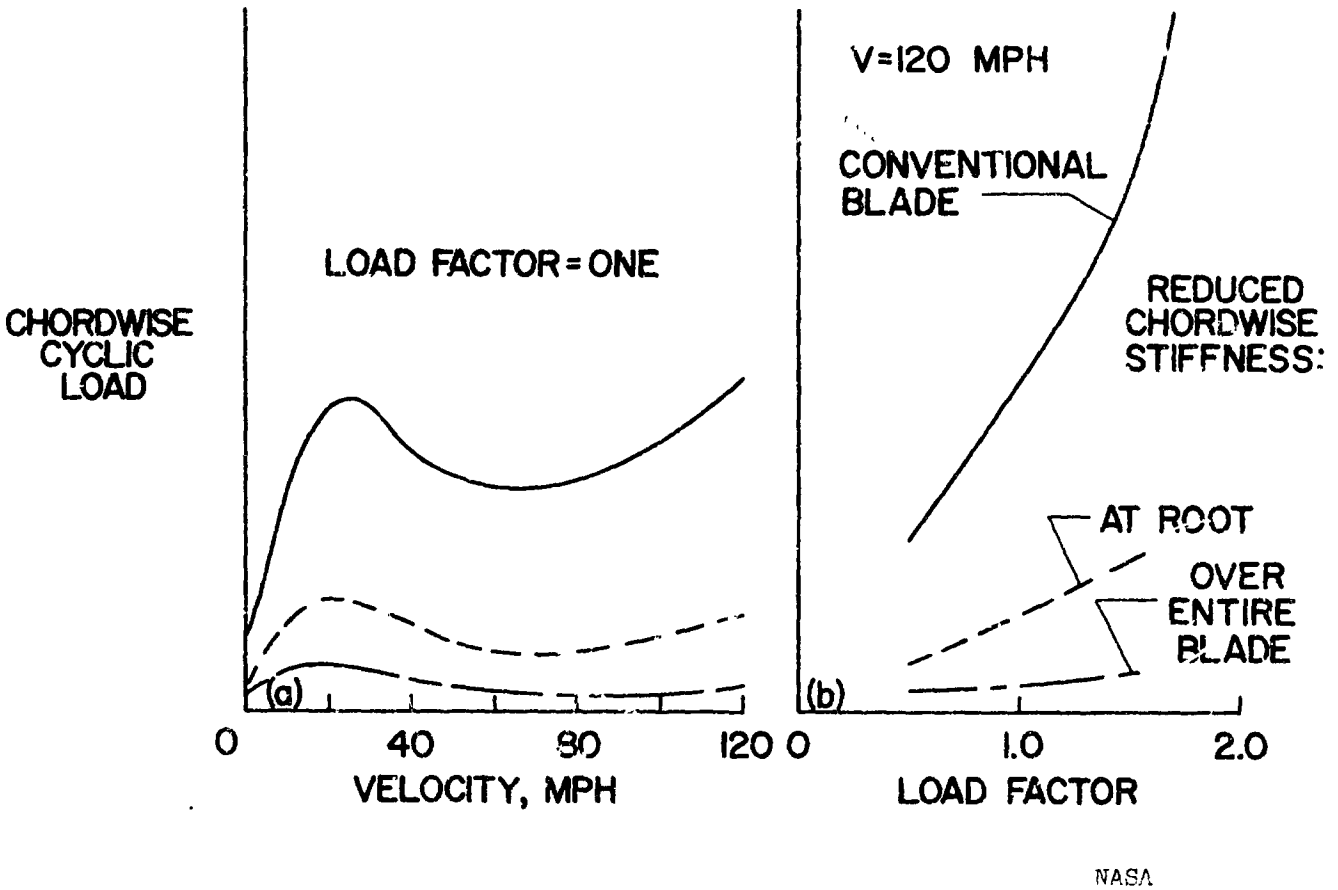

Figure 15.- Effect of blade chordwise stiffness on blade chordwise cyclic load.

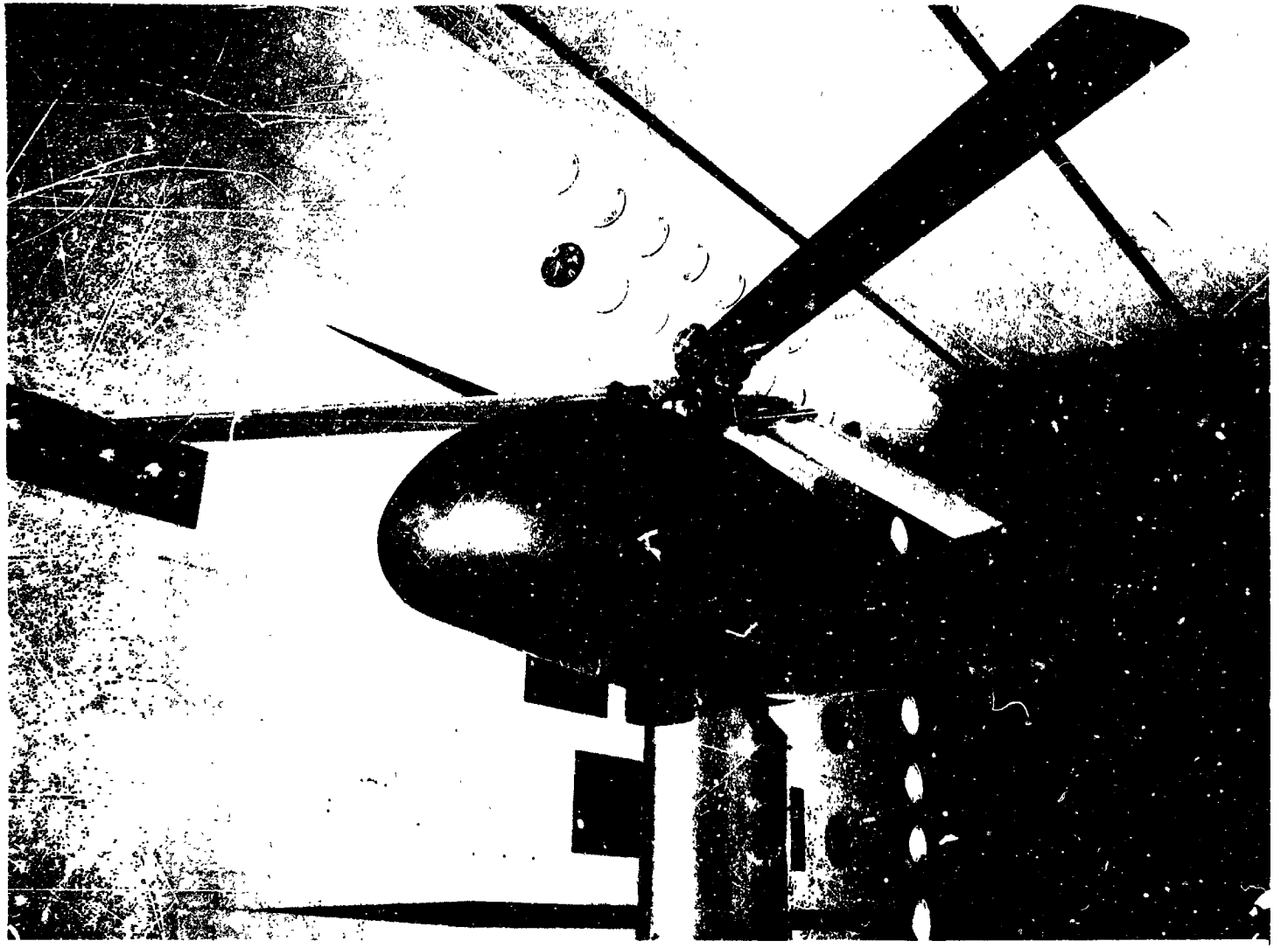

NASA

Figure 16.- Three-blade hingeless-rotor dynamic model in Langley 16-foot transonic dynamics tunnel. (Solidity = 0.12.)

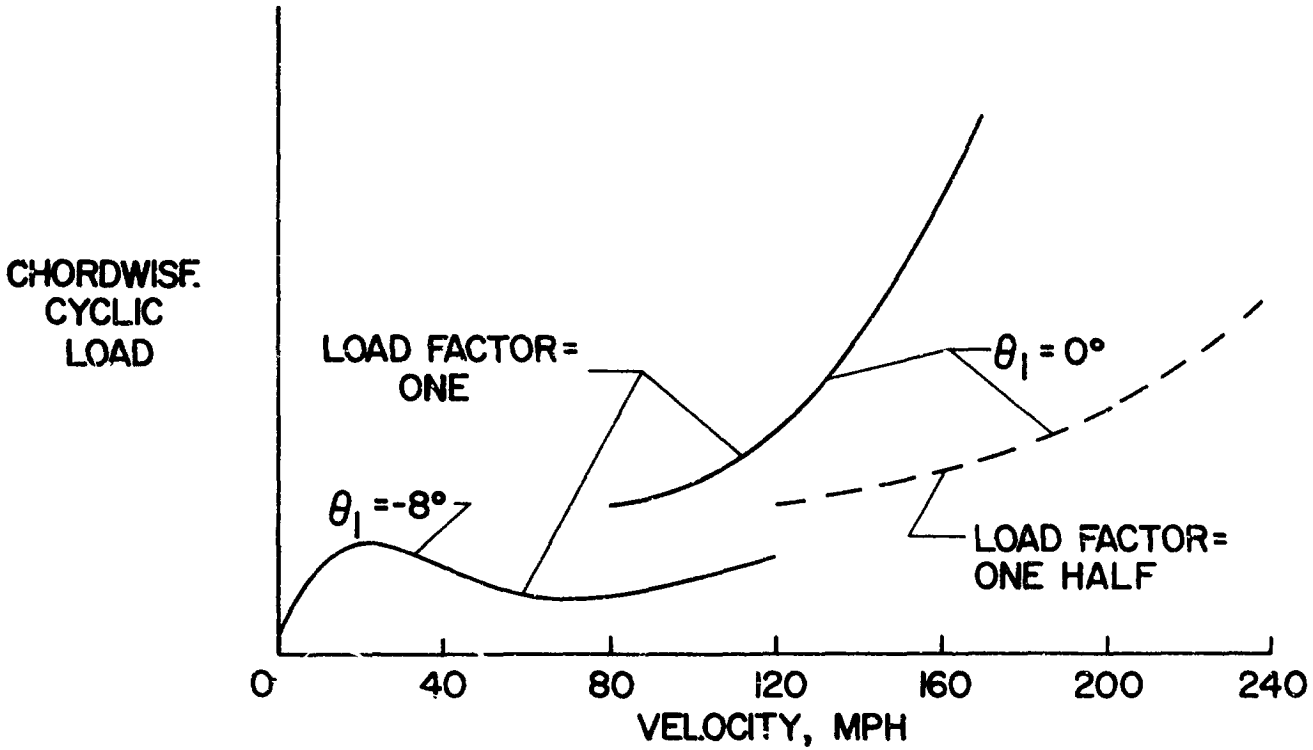

Figure 17.- Effect of load factor and blade twist on chordwise cyclic load.

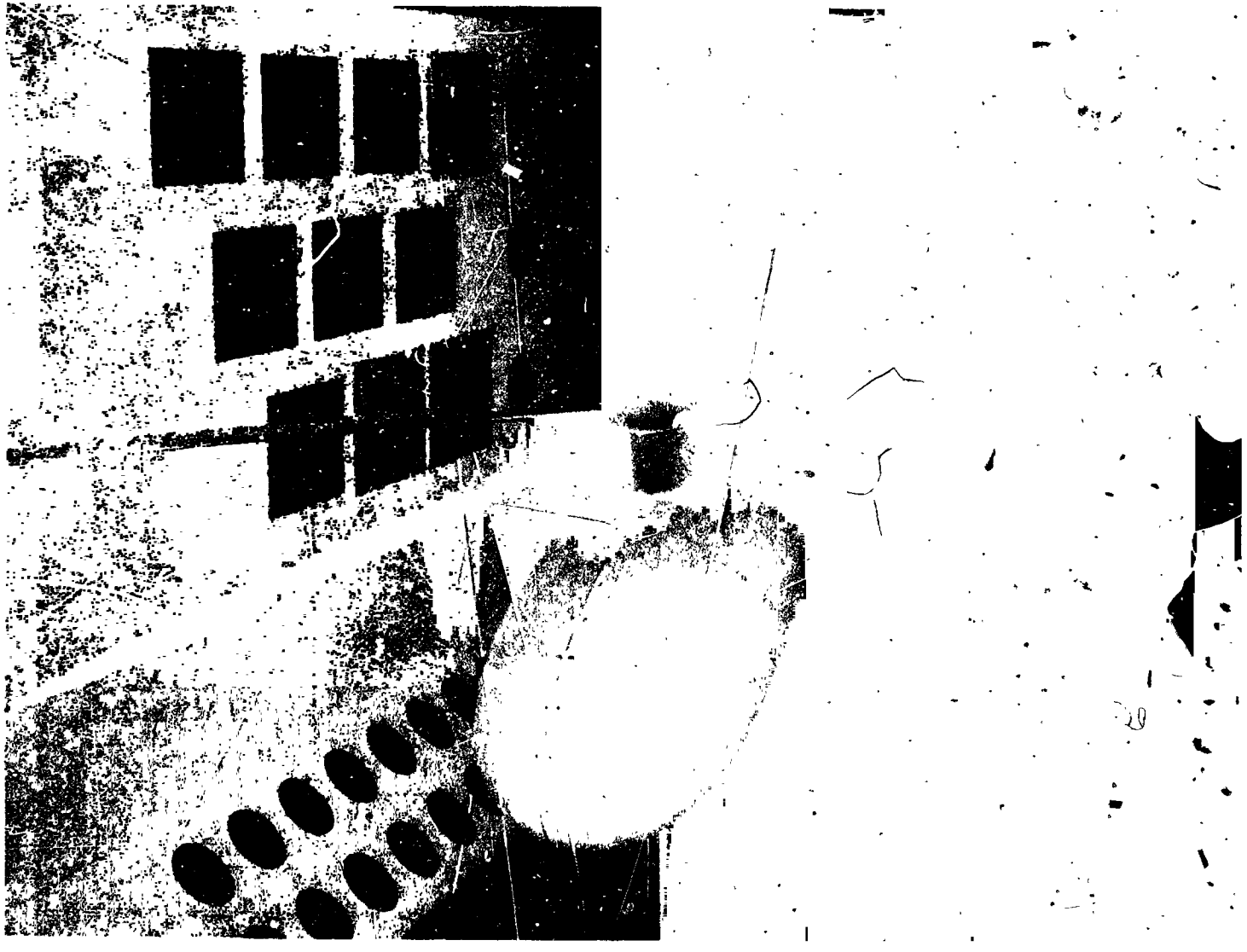

NASA

Figure 18.- Three-blade hingeless-rotor dynamic model in Langley 16-foot transonic dynamics tunnel. (Solidity = 0.06.)

NASA

Figure 19.- Four-blade hingeless-rotor dynamic model in Langley 16-foot transonic dynamics tunnel. (Solidity = 0.08.)